**This is a preprint version of the conference paper published in: Proceedings of the ASME 2023 International Mechanical Engineering Congress and Exposition. Volume 12: Micro- and Nano-Systems Engineering and Packaging. New Orleans, Louisiana, USA. October 29–November 2, 2023. V012T13A003. ASME.
https://doi.org/10.1115/IMECE2023-110762

PREPRINT: CHARACTERISTICS OF INPUT SIGNAL OF A XY AND YX CUT LINBO$_3$ SAW USING FINITE ELEMENT MODELING

Ranjith D. Janardhana [1] and Nathan Jackson [1,2]

[1]Department of Mechanical Engineering, University of New Mexico, Albuquerque, NM, USA
[2]Nanoscience and Microsystems Engineering, University of New Mexico, Albuquerque, NM, USA

ABSTRACT

Surface Acoustic Wave (SAW) devices were traditionally designed for wireless and communication applications, however their potential has been explored in various other fields. In recent years SAW devices have shown promising results in the area of acoustofluidics. SAW devices operate at higher frequencies (100's of MHz) which results in high propagation of mechanical waves on the surface which can be utilized in acoustofluidics applications such as cell separation and atomizer. Integration of SAW on acoustofluidics applications solely depends on the device's ability to generate an acoustic wave with high magnitude to transfer high levels of energy through the liquid. Various factors such as the shape of wave form and amplitude of the input signal to a SAW can affect the formation of mechanical waves on the surface. Hence, the performance of acoustofluidics applications mainly depends on the selection of input signal to a SAW device. This paper analyzes the characteristics of input signals such as the shape of impulse, signal timing, frequency range, and amplitude by considering piezoelectric substrate XY and YX cut $LiNbO_3$. The results were analyzed in relation to insertion loss which is an important parameter to determine the performance of the SAW device.

Keywords: SAW, Surface Acoustic Wave, Acoustofluidics, cell separation, pulse in SAW, insertion loss, MEMS, atomizer

NOMENCLATURE

C	elastic stiffness matrix
D	electric displacement
d	distance between IDTs
E	electrical field vector
e	piezoelectric constant
ϵ	permittivity matrix
f	frequency
IL	insertion loss
λ	wavelength, $\lambda = 2d$
ρ	density of mass
S	strain vector
T	stress vector
U_i	displacement components, $i = x, y, z$
V	electric potential
x_i	cartesian coordinate axis, $i = x, y, z$

1. INTRODUCTION

Acoustofluidics is an evolving lab-on-a-chip (LOC) technology in which fluid medium is excited by the high frequency propagating acoustic waves induced by the transducer. Cell sorting, particle separation, and atomization are some of the most popular and commonly used acoustofluidic applications [1–5]. These applications involve the formation of transverse mechanical waves on the surface of a piezoelectric device by applying an electrical signal to the Inter Digital Transducer (IDT) which acts as an electrode. Mechanical waves which interact with fluids are a combination of planar and transverse waves. The predominance of wave propagation direction depends on the crystal cut and orientation of the piezoelectric material due to its anisotropic properties [6]. $LiNbO_3$ is an often-found piezoelectric material which creates Surface Acoustic Wave (SAW) (frequently referred as Rayleigh Wave) on the surface that fades away along with the depth of a substrate that suits the acoustofluidics application [7,8].

The efficiency of the acoustofluidics device is simply dependent on the performance of the SAW device that ability to create the required high amplitude Rayleigh wave with minimum Insertion Loss (IL) [9]. Before integrating a SAW device with microfluidics there is a necessity to understand the propagation of the wavefront, operating frequency, IL, amplitude and velocity of the wave. These parameters are mainly dependent on the design of IDT, excitation/input signal and power, crystal cut and orientation and electromechanical coupling coefficient [10].

In this regard, the characteristics of SAW devices were investigated using time-dependent Finite Element Analysis (FEA) in COMSOL Multiphysics [11] commercial software. Initially, a two-dimensional (2D) $LiNbO_3$ substrate of size $1600\mu m \times 500\mu m$ with each of four electrodes as input and output was modeled. Initially, mesh sensitivity analysis was carried out for the verification of the Finite Element Model (FEM) on X cut Y propagating $LiNbO_3$. Later, the FEM model for X cut Y propagating $LiNbO_3$ was validated against experimental results [8] based on IL. The current study explored the characteristics of pulses by implementing various shapes of the input signal based on the applications of the pulse sequence reported in earlier studies [12–14]. The paper compares the effect

of the orientation of XY and YX cut $LiNbO_3$ substrate on insertion loss depending on pulses where SAW velocity for both cuts was reported around 3700m/s [15]. Further, this paper studied the effect of voltage on the displacement of the mechanical waves of the device as traveling SAW's (tSAW) and standing SAW's (sSAW) components was dependent on the voltage applied to IDTs [16].

2. MATERIALS AND METHODS

2.1 Model Equation

For a piezoelectric material the constitutive equation that couples between electric filed and strain [17] is given by

$$T_{ij} = C_{ijkl}\, S_{kl} - e_{kij} E_k \quad (1)$$

$$D_i = e_{ikl}\, S_{kl} - \epsilon_{ik} E_k \quad (2)$$

Further piezoelectric constitutive relation reduced to coupled wave equations [18] as follows,

$$-\rho \frac{\partial^2 u_i}{\partial t^2} + C_{ijkl} \frac{\partial^2 u_k}{\partial x_j \partial x_l} + e_{kij} \frac{\partial^2 V}{\partial x_k \partial x_j} = 0 \quad (3)$$

$$e_{ikl} \frac{\partial^2 u_k}{\partial x_i \partial x_l} - \epsilon_{ik} \frac{\partial^2 V}{\partial x_i \partial x_k} = 0 \quad (4)$$

with three degrees of freedom for displacement and one for electric potential.

2.2 Computational Domain

In this work, two different orientations: XY and YX cut $LiNbO_3$ were studied and the 2D computation model used in this study was represented in Fig. 1. Overall dimension of the domain consisting of $LiNbO_3$ substrate was $1600\mu m \times 500\mu m$. Two finger pairs of aluminum IDTs were considered at each input and output ports with a thickness $0.1\mu m$ and a width $10\mu m$. Input IDTs were named as "1", "2", "3" and "4" whereas output IDTs were "a", "b", "c" and "d". The periodicity of IDTs was $10\mu m$ $(\lambda/2)$. Distance of input IDT from output IDT was $90\mu m$.These computational domain dimensions were based on previously reported design [8].

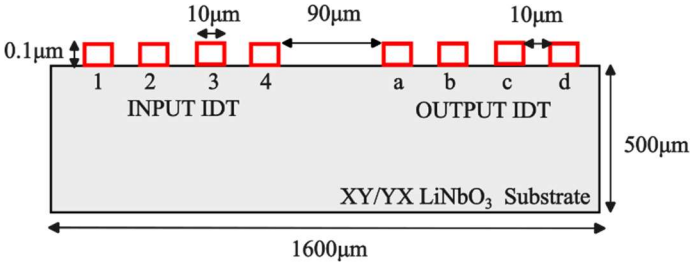

FIGURE 1. COMPUTATIONAL DOMAIN FOR SAW DEVICE.

2.2 Mesh and Boundary Conditions

Figures 2a and 2b show the example of the computational mesh with a zoomed view of area "A" near IDT. The quadrilateral mesh was applied for the entire domain by using the size and bias option near IDT regions as indicated in Fig. 2b. The mesh was divided into three structure blocks (Block 1, Block 2 and Block 3). Block 3 had finer mesh than block 1 and block 2. Mesh details were provided in Table 1.

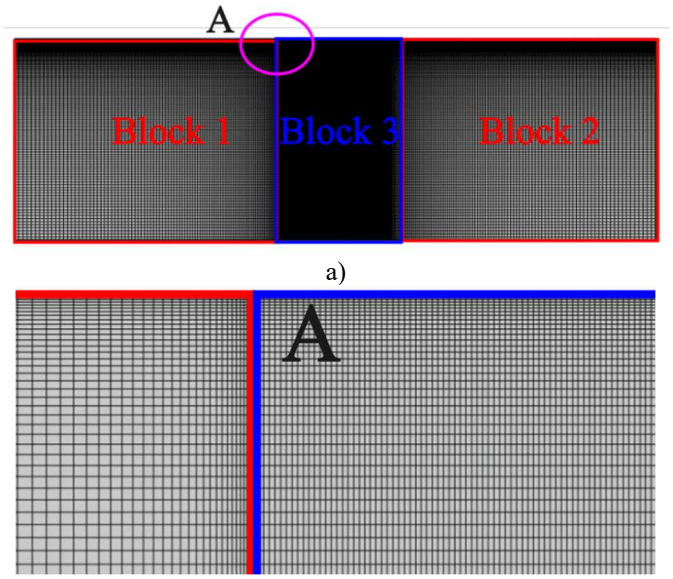

FIGURE 2. MESH FOR THE a) SAW DEVICE AND b) ZOOMED VIEW OF AREA "A" NEAR IDT.

TABLE 1. MESH DEATAILS.

	Number of Elements	Number of elements per wavelength (λ)
Element 1	31540	20
Element 2	60080	40
Element 3	88910	80
Element 4	146570	160
Element 5	204230	240

The left and right sides of the domain were enforced with periodic boundary conditions whereas the bottom of the domain kept fixed. The following impulse signal (V_i) was applied at input IDT as an initial condition for the characteristic study. Impulse function is applied to IDT fingers "2", "4" and "1", "3" (Fig. 1) were set 0V.

Step Pulse [19]:

$$V_i = \begin{cases} 1V, & 0 \le t \le 1ns \\ 0, & t \ge 1ns \end{cases} \quad (5)$$

Gaussian Pulse [20]:

$$V_i = \begin{cases} e^{-\frac{1}{2}(2\pi f \sigma)^2}, & 0 \le t \le 1ns \\ 0, & t \ge 1ns \end{cases} \quad (6)$$

Modified Gaussian Pulse [21]:

$$V_i = \begin{cases} e^{-(0.5\pi f_0 (t-T_0))^2} sin(2\pi f_0 (t - T_0), 0 \le t \le 1ns \\ 0, \quad t \ge 1ns \end{cases} \quad (7)$$

Sinusoidal Pulse [22]:

$$V_i = \begin{cases} sin(2\pi f_0 t - T_0), & 0 \le t \le 1ns \\ 0, & t \ge 1ns \end{cases} \quad (8)$$

Peak to peak sinusoidal voltage was applied at input IDT for voltage and displacement analysis. To determine open circuit voltage, output IDT (Fig. 1) was configured for the floating potential condition [19].

2.3 Crystal Orientation

Different orientation of the cut with respect to crystallographic axes changes the material properties such as elastic stiffness matrix (C), piezoelectric constant (e) and permittivity matrix (ϵ) due to anisotropic properties of $LiNbO_3$[23]. Orientation of the crystal cut was applied by rotating the coordinate system in COMSOL Multiphysics based on Euler angles. Additional details about rotating the coordinate system were provided in the COMSOL Multiphysics documentation [24]. XY cut $LiNbO_3$ specifies that the surface wave propagates in the Y direction normal to the X surface [22]. Correspondingly, YX cut $LiNbO_3$ indicates that the surface wave generated in the X direction was normal to the polarized Y direction. Euler angle was set to (0,90,0) [25] for XY cut $LiNbO_3$ for rotating the coordinate system in COMSOL whereas the default coordinate system was applied for YX cut $LiNbO_3$. Material properties for $LiNbO_3$ were set from the COMSOL material library and Table 2 describes properties for IDT.

TABLE 2. MATERIAL PROPERTIES OF IDT

Properties	Aluminum (IDT)
Young's Modulus (kPa)	70 x 10^9
Poisson's ratio	0.33
Density (kg/m^3)	2700

2.4 Numerical Simulation

Numerical analysis was conducted by FEM using COMSOL Multiphysics software to study the frequency response of the device by solving coupled 2D wave equations. Transient analyses were performed for a total time duration of 100 ns with time step 1ns (for verification) and 0.1ns (for rest) for different impulse functions (V_i) applied at input IDT as mentioned in equations (5) to (8). The impulse response of the system was recorded at output IDT. The frequency response of the device was obtained by performing Fast Fourier Transform (FFT) [8] by setting "Time to Frequency FFT" option in COMSOL. IL was calculated by the following expression [26],

$$IL = 20log_{10}\left|\frac{V_{output}}{V_i}\right| \quad (9)$$

Shape order for the dependent electric potential variable was considered quadratic on other hand two displacement variables was set as quadratic serendipity. Other solver parameters were set to COMSOL's default settings.

3 RESULTS AND DISCUSSION

Result section was divided into three sections: i) Verification and Validation ii) Characteristics of Pulses and iii) Voltage and Displacement.

3.1 Verification and Validation

A mesh independence study was performed for the XY cut $LiNbO_3$ using five different nodes as described in Table 1. Figure 4 illustrates the mesh sensitivity analysis results over different mesh sizes for time step 1ns. Three different frequencies were chosen: $f_a = 73.9\ MHz$, $f_b = 82.9\ MHz$ and $f_c = 92.3 MHz$ for mesh convergence study and results were depicted in Figs.5. The absolute error between "element 2" and "element 5" was within 1% (Fig. 5) as a result "element 2" (40 elements per wavelength) was chosen for all further simulations. Numerical results of XY cut $LiNbO_3$ was compared with the experimental outcomes to validate the model [8] as shown in Fig. 6.

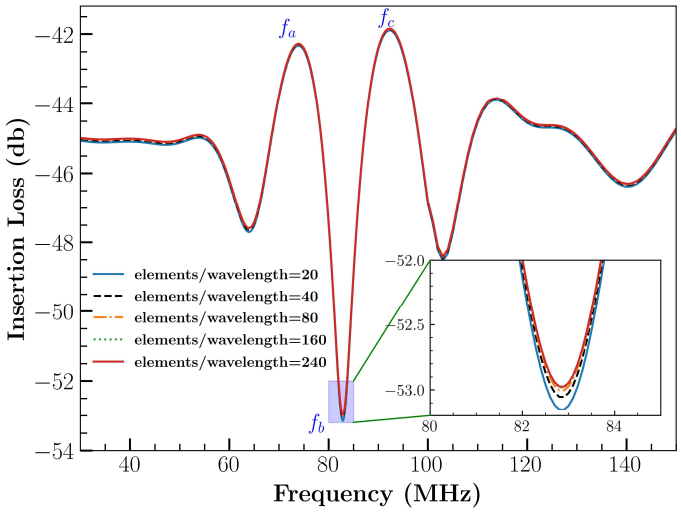

FIGURE 4. MESH SENSITIVITY ANALYSIS FOR DIFFERENT NUMBER OF ELEMENTS.

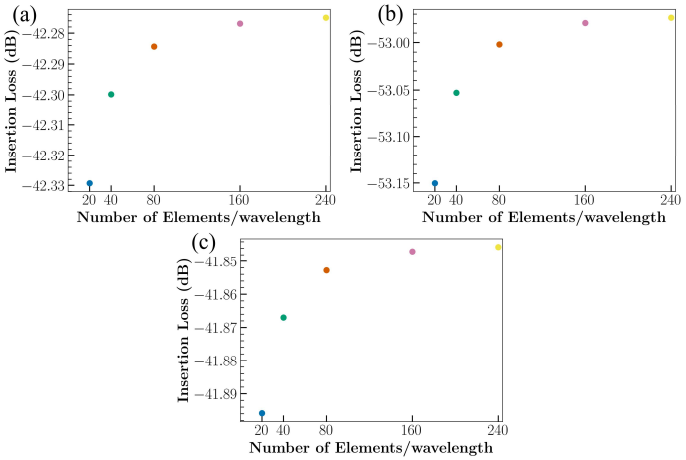

FIGURE 5. CONVERGENCE OF INSERTION LOSS AT LOCATION (a) f_a = 73.9 MHz, (b) f_b = 82.9 MHz, and (c) f_c = 92.3 MHz.

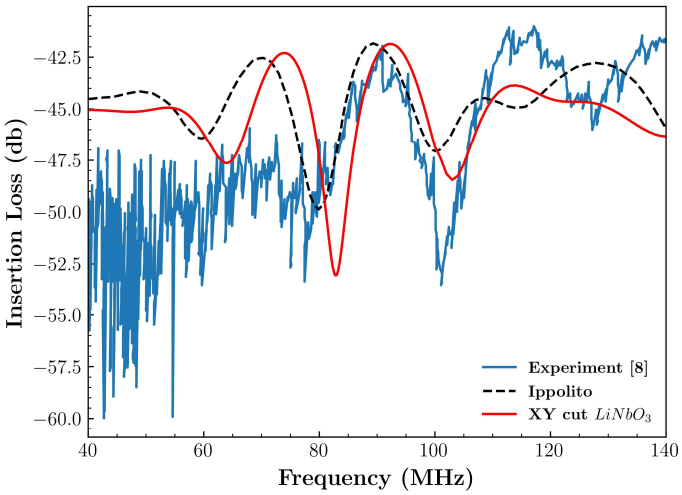

FIGURE 6. COMPARISION OF INSERTION LOSS WITH EXPERIMENTAL AND SIMUALTION RESULT FOR TIME STEP 0.1 ns.

Results obtained for IL were in good agreement with the experimental and simulation result [8] as displayed in Fig. 6. The shape of the input signal applied at the input IDT for equation (5) (Step pulse) used for the verification study for time step 0.1 ns was depicted in Fig. 7(a). The shape of the input signal was found to be noisy for time step 1 ns (Fig.7(b)), accordingly the time step 0.1 ns was used for the rest of the simulation due to the better representation of the input shape. IL result was displayed in Fig. 8 for XY cut LiNbO3 by implementing time step 1 ns. Conversely IL results of XY cut LiNbO3 with 0.1 ns (Fig. 6) time step resulted in better accuracy when compared to 1 ns.

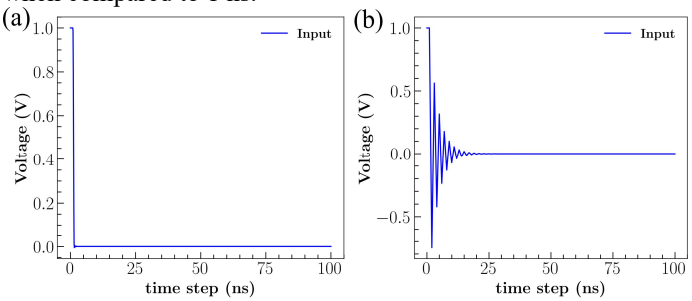

FIGURE 7. INPUT SIGNAL SHAPE AT INPUT IDT FOR (a) TIME STEP = 0.1 ns and (b) TIME STEP = 1 ns.

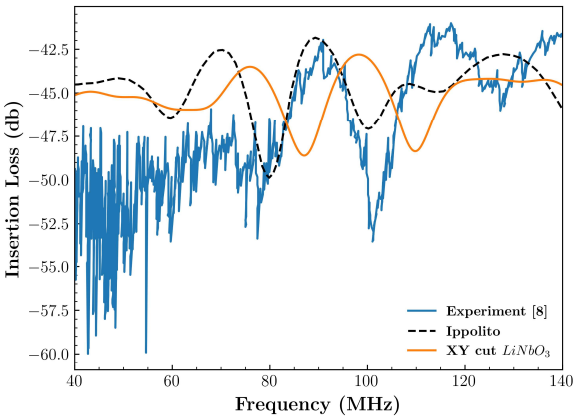

FIGURE 8. COMPARISION OF INSERTION LOSS WITH EXPERIMENTAL AND SIMUALTION RESULT OF XY CUT $LiNbO_3$ FOR TIME STEP 1 ns.

3.2 Characteristics of Pulses

This section describes and compares the characteristics of different shapes of pulses for XY and YX cut $LiNbO_3$ with shapes of the input signal with an amplitude of 1V.

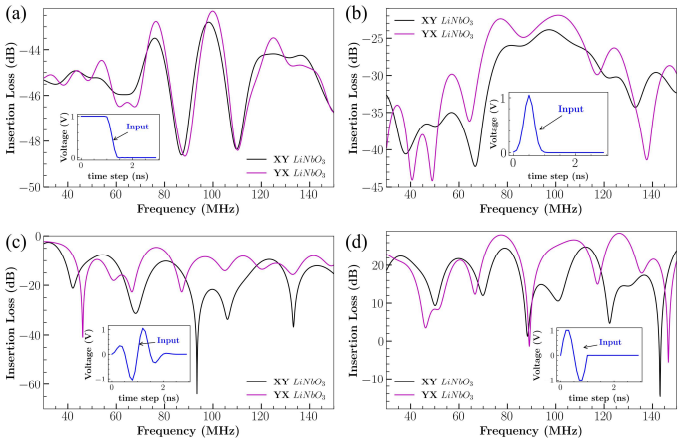

FIGURE 9. COMPARISION OF INSERTION LOSS OF XY CUT $LiNbO_3$ AND YX CUT $LiNbO_3$ FOR (a) STEP SHAPE PULSE, (b) GAUSSIAN SHAPE PULSE, (c) MODIFIED GAUSSIAN SHAPE, AND (d) SINUSOIDAL SHAPE PULSE.

Figure 9(a) shows the result of IL for XY and YX cut $LiNbO_3$ along with step pulse as an input signal. IL for YX cut $LiNbO_3$ is lower compared to XY cut $LiNbO_3$. Similarly, outcomes of IL were displayed in Fig. 9(b), (c) and (d) for Gaussian, modified Gaussian and sinusoidal shape pulses respectively. In all the case studies, the results of IL for YX cut $LiNbO_3$ were smaller in comparison with XY cut $LiNbO_3$. IL for the sinusoidal shape pulse was found to be lower compared to the other input waveforms. Therefore, the next section analyzes the effect of applying continuous sinusoidal signal by varying peak-to-peak voltage to study the displacement of mechanical waves.

3.3 Voltage and Displacement

Figures 10 and 11 illustrates the comparison of displacement components U_x and U_y at location "j" (Fig. 1) depending on the coordinate axis for XY and YX cut $LiNbO_3$ by varying the peak-to-peak sinusoidal voltage. The displacement increased for all cases with increment in voltage. The magnitude of transverse component normal to the surface was found to be dominant in both XY and YX cut $LiNbO_3$ as shown in Figs. 10 and 11.

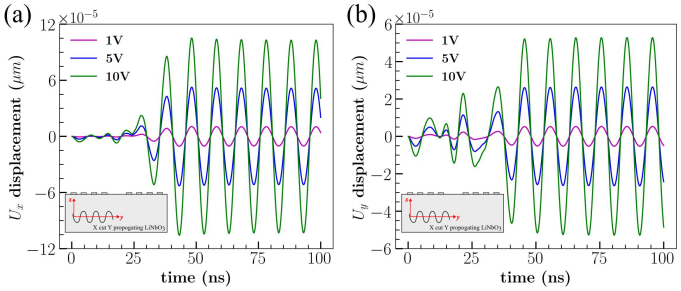

FIGURE 10. COMPARISION OF DISPLACEMENT (a) U_x AND (b) U_y AT DIFFERENT VOLTAGES FOR XY CUT $LiNbO_3$.

The dominance of the transverse components was reported in previous studies [7,8]. In comparison to XY cut $LiNbO_3$, displacement of the transverse component was moderately higher for YX cut $LiNbO_3$ (Fig. 11). However, for YX cut $LiNbO_3$ (Fig. 19), the effect of the longitudinal component along the wave propagation was also maximal. As result, both XY and YX cut $LiNbO_3$ produce a combination of the transverse and longitudinal wave with dominance in out-of-plane direction.

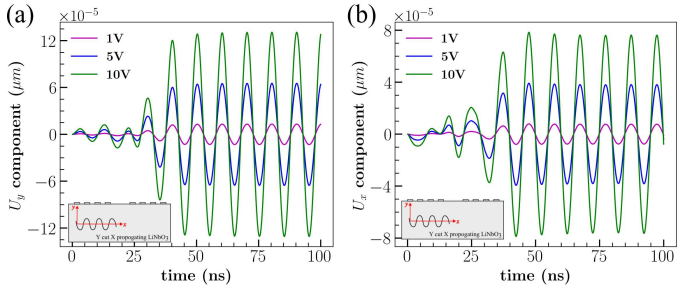

FIGURE 11. COMPARISION OF DISPLACEMENT (a) U_y AND (b) U_x AT DIFFERENT VOLTAGES FOR YX CUT $LiNbO_3$.

Figure 12 compares the displacement components U_x and U_y at 1V for XY cut $LiNbO_3$. Similar outcomes were described where displacements components (U_x and U_y) were out of phase with each other [7]. Total displacement surface plots that represent the wavefront formation for XY and YX cut $LiNbO_3$ were shown in Figs. 13 for 1V at time 100ns. Figures 13 show that the wavefront shape varies depending on crystal orientation. According to a previous study, increased excitation power could cause the device to overheat [27]. Conversely alternative approaches might involve using the sequence of pulse voltage for a small duration as outlined in section 3.2.

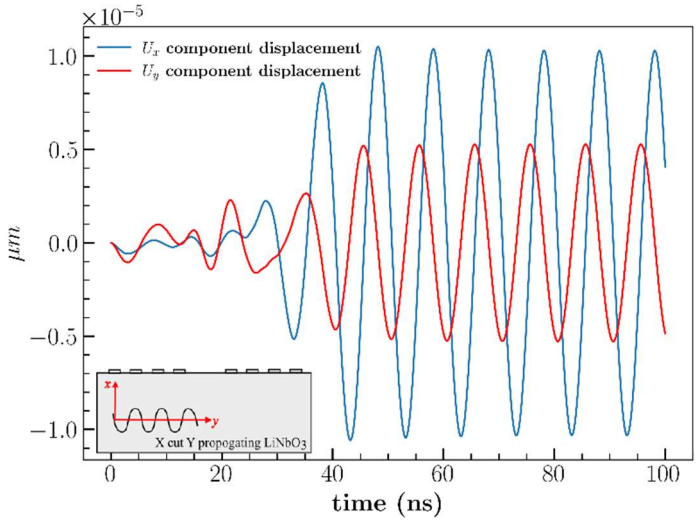

FIGURE 12. COMPARISION OF DISPLACEMENT COMPONENTS U_x AND U_y AT 1 V FOR XY CUT $LiNbO_3$.

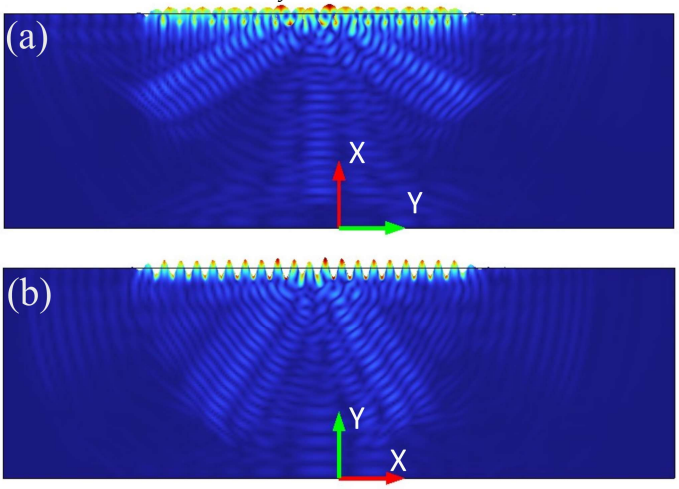

FIGURE 13. SURFACE PLOT OF TOTAL DISPLACEMENT FOR (a) XY CUT AND (b) YX CUT $LiNbO_3$ AT TIME=100ns FOR 1V (DISPLACMENT SCALE RATIO=1.5× $10^6 \mu m$).

4 CONCLUSION

In this framework, the 2D FEM model of XY cut $LiNbO_3$ was verified and validated with experimental result [8]. However, the representation of the input signal was found to be noisy for time step 1ns. Reduction of time step to 0.1ns retained the shape of the input signal as represented in Figs. 9 and 10. The previous study [28] reported that the inclusion of the "z" direction (3D model) would improve the result of IL for XY cut $LiNbO_3$. Various shapes of impulse such as sinusoidal, Gaussian pulse, modified Gaussian and step pulses were studied, and respective output characteristics for XY and YX cut $LiNbO_3$ devices were measured. These output characteristics were represented as insertion loss in Figs. 12, 13, 14 and 15. Within a higher operating frequency of 80-100 MHz, the IL was minimum for YX cut in comparison with XY cut $LiNbO_3$. Based on the minimum IL for a sinusoidal pulse from the characteristics study, the effect of excitation voltage on the displacement of the device was analyzed and results were depicted in Figs. 10 and 11. The

outcome demonstrated that wavefront was a combination of transverse and longitudinal wave components with dominance in the transverse direction normal to the wave propagation. The displacement component in direction of wave propagation was found to be of lesser magnitude in the case of XY cut $LiNbO_3$ (Fig. 10). Surface plots for total displacement (Figs. 13) illustrate that the orientation of the crystal influences the wavefront formation.

From the above analysis, the selection of an input signal to SAW is crucial for achieving higher efficiency of acoustofluidics based SAW devices depending on operating frequency, IDT design, excitation power and piezoelectric material properties. Future work would involve a series of experiments to validate the FEM simulation by integrating with microfluidics and optimizing the FEM model by considering the wave effects in 3D.

ACKNOWLEDGEMENTS

The authors would like to thank all members of the SMART Laboratory group at University of New Mexico.

REFERENCES

[1] Destgeer, G., and Sung, H. J., 2015, "Recent Advances in Microfluidic Actuation and Micro-Object Manipulation via Surface Acoustic Waves," Lab Chip, **15**(13), pp. 2722–2738.

[2] Franke, T., Abate, A. R., Weitz, D. A., and Wixforth, A., 2009, "Surface Acoustic Wave (SAW) Directed Droplet Flow in Microfluidics for PDMS Devices," Lab Chip, **9**(18), p. 2625.

[3] Winkler, A., Bergelt, P., Hillemann, L., and Menzel, S., 2016, "Influence of Viscosity in Fluid Atomization with Surface Acoustic Waves," OJA, **06**(03), pp. 23–33.

[4] Ding, X., Peng, Z., Lin, S.-C. S., Geri, M., Li, S., Li, P., Chen, Y., Dao, M., Suresh, S., and Huang, T. J., 2014, "Cell Separation Using Tilted-Angle Standing Surface Acoustic Waves," Proc. Natl. Acad. Sci. U.S.A., **111**(36), pp. 12992–12997.

[5] Zhang, S. P., Lata, J., Chen, C., Mai, J., Guo, F., Tian, Z., Ren, L., Mao, Z., Huang, P.-H., Li, P., Yang, S., and Huang, T. J., 2018, "Digital Acoustofluidics Enables Contactless and Programmable Liquid Handling," Nat Commun, **9**(1), p. 2928.

[6] Wu, M., Ozcelik, A., Rufo, J., Wang, Z., Fang, R., and Jun Huang, T., 2019, "Acoustofluidic Separation of Cells and Particles," Microsyst Nanoeng, **5**(1), p. 32.

[7] Kannan, T., "Finite Element Analysis of Surface Acoustic Wave Resonators," p. 129.

[8] Ippolito, S. J., "A Thesis Submitted in Fulfilment of the Requirements for the Degree of Doctor of Philosophy."

[9] Connacher, W., Zhang, N., Huang, A., Mei, J., Zhang, S., Gopesh, T., and Friend, J., 2018, "Micro/Nano Acoustofluidics: Materials, Phenomena, Design, Devices, and Applications," Lab Chip, **18**(14), pp. 1952–1996.

[10] Mandal, D., and Banerjee, S., 2022, "Surface Acoustic Wave (SAW) Sensors: Physics, Materials, and Applications," Sensors, **22**(3), p. 820.

[11] "COMSOL Multiphysics® v. 6.1."

[12] Riaud, A., Baudoin, M., Thomas, J.-L., and Matar, O. B., 2016, "SAW Synthesis with IDTs Array and the Inverse Filter: Toward a Versatile SAW Toolbox for Microfluidics and Biological Applications."

[13] Daw, J., Deng, Z., and Palmer, S., "Characterization of Advanced Manufactured Surface Acoustic Wave Sensors for Temperature Measurement in Nuclear Applications."

[14] Horesh, A., Connacher, W., and Friend, J., 2023, "Acoustothermal Phase Change and Acoustically Driven Atomization for Cold Liquid Microthrusters," Appl. Phys. Lett., **122**(1), p. 014104.

[15] Ciplys, D., and Rimeika, R., 1999, "Measurements of Electromechanical Coupling Coefficient for Surface Acoustic Waves in Proton-Exchanged Lithium Niobate," pp. 14–20.

[16] Devendran, C., Gunasekara, N. R., Collins, D. J., and Neild, A., "Batch Process Particle Separation Using Surface Acoustic Waves (SAW): Integration of Travelling and Standing SAW," RSC Advances.

[17] Vellekoop, M. J., 1997, "Acoustic Wave Sensors. Theory, Design and Physicochemical Applications," Sensors and Actuators A: Physical, **63**(1), p. 79.

[18] Guanshui Xu, 2000, "Finite Element Analysis of Second Order Effects on the Frequency Response of a SAW Device," *2000 IEEE Ultrasonics Symposium. Proceedings. An International Symposium (Cat. No.00CH37121)*, IEEE, San Juan, Puerto Rico, pp. 187–190.

[19] Kabir, K. M. M., Matthews, G. I., Sabri, Y. M., Russo, S. P., Ippolito, S. J., and Bhargava, S. K., 2016, "Development and Experimental Verification of a Finite Element Method for Accurate Analysis of a Surface Acoustic Wave Device," Smart Mater. Struct., **25**(3), p. 035040.

[20] Balistreri, R., 2017, "Loudspeaker Response Optimization with the Aid of Impulse Response."

[21] Prinn, A. G., 2021, "On Computing Impulse Responses from Frequency-Domain Finite Element Solutions," J. Theor. Comp. Acout., **29**(01), p. 2050024.

[22] Xu, G., 2000, "Direct Finite-Element Analysis of the Frequency Response of a *Y* - *Z* Lithium Niobate SAW Filter," Smart Mater. Struct., **9**(6), pp. 973–980.

[23] Zhang, G., "Orientation of Piezoelectric Crystals and Acoustic Wave Propagation," p. 18.

[24] Datta, S., "Piezoelectric Materials: Crystal Orientation and Poling Direction," Piezoelectric Materials: Crystal Orientation and Poling Direction.

[25] Namnabat, M. S., Moghimi Zand, M., and Houshfar, E., 2021, "3D Numerical Simulation of Acoustophoretic Motion Induced by Boundary-Driven Acoustic Streaming in Standing Surface Acoustic Wave Microfluidics," Sci Rep, **11**(1), p. 13326.

[26] Rao, Y. L., "NANOSTRUCTURE-ENHANCED SURFACE ACOUSTIC LOVE WAVE DEVICES FOR BIOSENSING APPLICATIONS."

[27] Cui, M., Kim, M., Weisensee, P. B., and Meacham, J. M., 2021, "Thermal Considerations for Microswimmer Trap-and-Release Using Standing Surface Acoustic Waves," Lab Chip, **21**(13), pp. 2534–2543.

[28] Ippolito, S. J., Kalantar-Zadeh, K., Powell, D. A., and Wlodarski, W., 2003, “A 3-Dimensional Finite Element Approach for Simulating Acoustic Wave Propagation in Layered SAW Devices,” *IEEE Symposium on Ultrasonics, 2003*, IEEE, Honolulu, HI, USA, pp. 303–306.